

New challenges for Adaptive Optics: Extremely Large Telescopes

M. Le Louarn^{1,2*} N. Hubin¹ M. Sarazin¹ A. Tokovinin¹

¹ *European Southern Observatory, Karl Schwarzschild Str. 2 - D-85748 Garching, Germany*

² *CRAL - Observatoire de Lyon, 9, Av. Charles André - F-69561 Saint Genis Laval, France*

Accepted 1999 November 3. Received 1999 November 4; in original form 1999 November 3

ABSTRACT

The performance of an adaptive optics (AO) system on a 100 m diameter ground based telescope working in the visible range of the spectrum is computed using an analytical approach. The target Strehl ratio of 60 % is achieved at 0.5 μm with a limiting magnitude of the AO guide source near $R \sim 10$, at the cost of an extremely low sky coverage. To alleviate this problem, the concept of tomographic wavefront sensing in a wider field of view using either natural guide stars (NGS) or laser guide stars (LGS) is investigated. These methods use 3 or 4 reference sources and up to 3 deformable mirrors, which increase up to 8-fold the corrected field size (up to 60'' at 0.5 μm). Operation with multiple NGS is limited to the infrared (in the J band this approach yields a sky coverage of 50 % with a Strehl ratio of 0.2). The option of open-loop wavefront correction in the visible using several bright NGS is discussed. The LGS approach involves the use of a faint ($R \sim 22$) NGS for low-order correction, which results in a sky coverage of 40 % at the Galactic poles in the visible.

Key words: Instrumentation: adaptive optics – Atmospheric effects – Telescopes

1 INTRODUCTION

The current generation of large ground based optical telescopes has a diameter of the primary mirror in the 8 to 10 metre range. Recently some thoughts have been given to the next generation optical telescopes on the ground. In these projects the diameter of the primary mirror lies in a range between 40 and 100 metres (see Gilmozzi et al. 1998, Andersen et al. 1999, Mountain 1997). The use of Adaptive Optics (AO, Roddier 1999) in the visible is crucial to obtain the full potential in angular resolution, to avoid source confusion for extragalactic studies at high redshifts, and to reduce the background contribution, dramatically increasing limiting magnitude (the signal to noise ratio is then proportional to the square of telescope diameter). Competition with space based observatories, providing diffraction limited imaging on an 8 m class telescope (see Stockman 1997) is also a driver for AO correction in the visible with larger apertures.

In this paper we address key issues for a visible light AO system on these Extremely Large Telescopes (ELTs). We have chosen a telescope diameter of 100 m, since it represents

the extreme case and we want to investigate the limiting factors of AO on such a large aperture. We shall not address here the astrophysical drivers for such aperture size, which are presented elsewhere (Gilmozzi et al. 1998). We model the performance of an AO system working in the visible on a 100 m telescope, for an on-axis natural guide star (NGS) (section 2). The sky coverage with this approach is close to zero, because only bright objects ($R \sim 10$) can be used as AO reference. The use of a single artificial laser guide star (LGS) is ruled out by the huge error introduced by the cone effect or focus anisoplanatism (Foy & Labeyrie 1985). We propose to use turbulence tomography (i.e. 3D mapping of turbulence, Tallon & Foy 1990, hereafter TF90) combined with Multi-Conjugate Adaptive Optics (Foy & Labeyrie 1985, Beckers 1988, hereafter MCAO) as a way to increase the fraction of the sky which can be observed. In section 3 we present the main concepts involved in turbulence tomography. In section 4 we describe a fundamental limitation of the corrected field of view size corrected by a small (1-3) number of deformable mirrors (DMs) and taking into account real turbulence profiles. A solution using 3 NGSs is presented, where the correction is done in the visible (section 5) and in the near-infrared (section 6). In section 7, another solution is presented, based on 4 LGSs for visible correction. In the following section, we present and quantify some technical as-

* e-mail: lelouarn@eso.org (MLL), nhubin@eso.org (NH), msarazin@eso.org (MS), atokovin@eso.org (AT)

pects of AO on ELTs. Finally, in section 9, the conclusions are given.

2 AO PERFORMANCE WITH AN ON-AXIS NGS

There is a strong scientific interest in visible light studies with the ELTs. Using the software described in Le Louarn et al. (1998) to perform analytical calculations of the AO system performance, we modeled a system with a Strehl ratio (ratio of the peak intensity of the corrected image to the peak intensity of a diffraction limited image, hereafter SR) of 60 % at $0.5 \mu\text{m}$, based on a Shack-Hartmann wavefront sensor (e.g. Rousset 1994). The target SR is higher than required by the scientific goals, $\sim 40 \%$, to take into account potential error sources arising outside the AO system (e.g. aberration of the optics or co-phasing errors of the telescope primary mirror segments). Considering the current performance of AO systems, this is a challenging goal. However, the start of the operation of ELTs is planned in 10-20 years from now, and AO technology is bound to evolve considerably. The atmospheric model we used in these calculations corresponds to good observing conditions at Very Large Telescope observatory of Cerro-Paranal in Chile (Le Louarn et al. 1998). The main atmospheric parameters and the AO hardware characteristics are summarized in Tab. 1.

The effects of scintillation on the wavefront sensing were neglected. Preliminary studies (Rousset 1999, private communication) have shown that the wavefront error contribution could be between 20 and 30 nm rms, reducing the SR by $\sim 10 \%$. The effects of the outer scale of turbulence were also neglected. Measurements (Martin et al. 1998) yield values usually between 20 to 30 m, significantly smaller than the diameter of the ELT. This is a new situation compared to current large telescopes. The effect of the outer scale is mainly to reduce the relative contribution of low order modes of wavefront distortions (Sasiela 1994) and to decrease the stroke needed for the DM to several microns, independently of telescope diameter. This relaxes constraints on the design of DMs, but does not change the overall on-axis system performance.

The simulation results are presented in Fig. 1. The target SR of 60 % is obtained in the visible, providing 1.03 milli-arcsecond (mas) diffraction limit at $0.5 \mu\text{m}$. The peak SR is over 95 % in K band ($2.2 \mu\text{m}$), the diffraction limit being 4.5 mas. Due to the fine wavefront sampling needed for correction in the visible, the limiting magnitude (at $0.5 \mu\text{m}$) is $R \sim 10$, which is bright compared to current AO systems working in the near-infrared (around $R \sim 16$, e.g. Graves et al. 1998). This implies that with a single NGS the sky coverage is extremely small (see Rigaut & Gendron 1992, Le Louarn et al. 1998 for a more extensive discussion on sky coverage with AO systems).

To overcome this limitation, we propose two different options, both involving multiple reference sources: NGS and LGS approaches are investigated in the following sections.

Table 1. AO simulation parameters. Atmospheric values are given at $0.5 \mu\text{m}$, WFS = wavefront sensor.

Telescope diameter	100 m
Number of actuators	~ 500000
WFS readout noise	$1 e^-$
WFS quantum efficiency	90 %
WFS spectral bandwidth	500 nm
Transmission ¹	40 %
WFS subaperture size	16 cm
Max. WFS sampling rate	500 Hz
Seeing	$0.5''$
Coherence time	6 ms
Isoplanatic angle	$3.5''$

¹Transmission of the atmosphere and telescope optics to the wavefront sensor. For visible light observations, light must be split between the wavefront sensor path and imaging path.

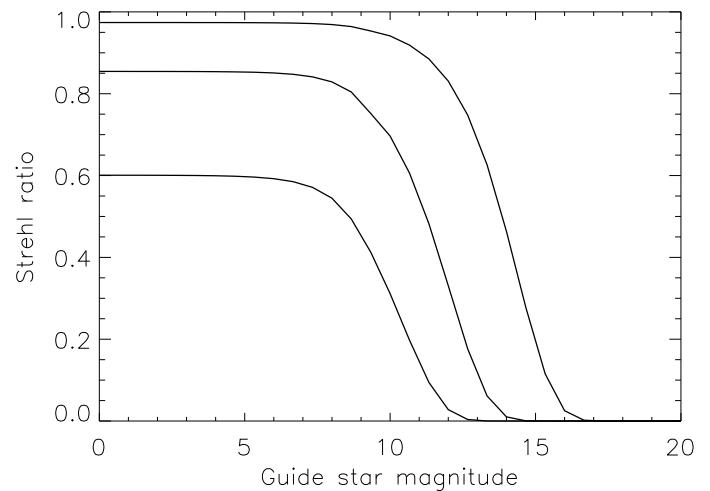


Figure 1. Strehl ratio versus magnitude at 0.5 , 1.25 and $2.2 \mu\text{m}$ (from bottom curve to top) for one on-axis NGS with the telescope pointing at zenith

3 TURBULENCE TOMOGRAPHY

Turbulence tomography is a technique to measure the wavefront corrugations produced by discrete atmospheric turbulent layers with the help of several reference sources (TF90). Assuming weak turbulence, the phase corrugations produced by each layer add linearly (Roddier 1981). Knowing the configuration of the guide sources (position in the sky, height above ground in the case of an artificial star) and the altitudes of the layers to be measured, it is possible to reconstruct the phase at the selected turbulent layers. Foy & Labeyrie (1985) proposed to use Multiple DMs to correct them individually, a concept called Multi-Conjugate AO (MCAO). There must be at least as many measurements (number of guide stars times number of measurements points on the pupil) as there are unknowns (number of corrected layers times actuators on the correcting mirrors). Therefore, only a small number (2-4) of turbulent layers can be reconstructed, if a small number (~ 4) of reference sources are to be used. Recent papers have tackled the problems of turbulence tomography (TF90, Tallon et al. 1992, Ragazzoni et al. 1999, Fusco et al. 1999, Le Louarn & Tal-

lon 2000), and reconstruction of turbulent wavefronts has been demonstrated in numerical simulations.

The maximum size θ of the tomographic corrected Field of View (FOV) is given by geometrical considerations:

$$\theta = \frac{D}{h_{max}} \left(1 - \frac{h_{max}}{H}\right), \quad (1)$$

where D is the diameter of the telescope, h_{max} is the height of the highest turbulent layer and H the height of the guide star (infinity for a NGS). As pointed out by TF90, in circular geometry, a small fraction of turbulence is not probed with this maximum FOV (pupil plane vignetting). This problem can be alleviated with a modal approach to turbulence tomography, which allows a slight interpolation of the wavefront within the corrected FOV (Fusco et al. 1999). With a 100 m telescope it may be possible to search reference stars in a much larger patch of the sky than with an 8 m class telescopes. The probability to find a references source can be dramatically increased (Ragazzoni 1999). For a 100 m telescope, the maximum tomographic field is $17'$ in diameter with a NGS, or $13'$ for LGSs, if the highest turbulent layer is at 20 km above ground.

The image is corrected in the whole tomographic FOV only if the whole turbulence is concentrated in few thin layers and if each layer is optically conjugated to its correcting mirror. Taking into account real turbulence profiles, we compute in the next section the FOV size which can be corrected with few DMs and we show that it is much less than the tomographic FOV.

4 LIMITATIONS OF MULTI-CONJUGATE AO

4.1 Turbulence vertical profile measurements

We have analyzed the PARSCA (Paranal Seeing Campaign, Fuchs & Vernin 1993) balloon data on the vertical distribution of turbulence to test the assumption that all turbulence is concentrated within a few layers. During the site testing campaign, 12 balloons were launched at night-time to measure the profile of the refraction index constant, $C_n^2(h)$. SCIDAR (Scintillation Detection and Ranging, Azouit & Vernin 1980) measurements were also made simultaneously, confirming the balloon soundings (Sarazin 1996).

In Tab. 2 we summarize some parameters of the balloon flights. The average Fried parameter (Fried 1966), r_0 , was 19 cm at $0.5 \mu\text{m}$, corresponding to a seeing of $0.55''$ —slightly better than the average seeing at Paranal, $0.65''$. Considering the small time span during which the balloons were launched (19 days), these data are not fully representative of the site. The parameters have been corrected for the height difference between the observatory (2638 m), and the launching site (2500 m), which explains the slight difference with other publications (e.g. Sarazin 1996).

In Fig. 2 the C_n^2 profiles obtained by the balloon flights are plotted. The height resolution of the balloons is ~ 5 m. For clarity these measurements have been convolved with a Gaussian of standard deviation 500 m. The physics and formation of very thin turbulence laminae is described in Coulman et al. 1995. For most of the flights the thin turbulent layers form larger structures which can be identified with the turbulent layers seen by SCIDAR (see for example the concentration of turbulence near 15 km on flight 45, altitudes

Table 2. Balloon data for Cerro Paranal. The atmospheric coherence length, r_0 and the isoplanatic angle θ_0 , are given at a wavelength of $0.5 \mu\text{m}$.

Flight	Date	Time	r_0 (m)	θ_0 (")
38	10.03.92	3:30	0.32	3.80
39	11.03.92	4:45	0.15	4.09
40	12.03.92	1:30	0.21	3.58
43	14.03.92	2:45	0.07	0.42
45	15.03.92	1:00	0.19	2.05
46	15.03.92	5:00	0.22	1.74
48	16.03.92	4:10	0.17	2.48
50	24.03.92	8:12	0.13	1.66
51	25.03.92	2:43	0.23	2.03
52	25.03.92	7:11	0.21	2.22
54	23.03.92	4:10	0.22	2.81
55	29.03.92	9:15	0.14	1.65

are expressed in kilometres above sea level). The strongest of these layers is the boundary layer, in the first kilometres of the atmosphere, present on all plots. Another layer, present on most flights, is located near 10-12 km. These measurements confirm the existence of numerous layers. However, a continuous component of small but significant amplitude is also present on most of the soundings.

4.2 Anisoplanatism in MCAO

We used the high resolution profiles (not convolved with a Gaussian) and applied the analytical formula derived by Tokovinin, Le Louarn, & Sarazin (2000) to calculate the size of the FOV θ_M which can be corrected with M deformable mirrors. This is a generalized isoplanatic angle in the sense of Fried (1982), expressed as

$$\theta_M = \left[2.905(2\pi/\lambda)^2 \times \int C_n^2(h) F_M(h, H_1, H_2, \dots, H_M) dh \right]^{-3/5}, \quad (2)$$

where F_M is a function depending on the conjugation heights of the DMs, H_i the height of conjugation, above ground. This expression assumes that the correction signals applied to each DM are optimized. It assumes an infinite turbulence outer scale and an infinite D/r_0 ratio. For 1 DM conjugated to altitude H_1 , Eq. 2 contains:

$$F_1(h) = |h - H_1|^{5/3}, \quad (3)$$

which reduces to $F_1(h) = h^{5/3}$ if $H_1 = 0$ as in conventional AO and yields the classical θ_0 . For a two mirror configuration the function has the form:

$$F_2(h, H_1, H_2) = 0.5 \left[|h - H_1|^{5/3} + |h - H_2|^{5/3} - 0.5|H_2 - H_1|^{5/3} - 0.5|H_2 - H_1|^{-5/3} (|h - H_1|^{5/3} - |h - H_2|^{5/3})^2 \right] \quad (4)$$

For 3 or more DMs the expression for F_M is much more complex. The heights H_i were computed with a multi-parameter optimization algorithm to maximize θ_M . We explored the possibilities with 1, 2 and 3 DMs in different altitude combinations, from all H_i fixed to all H_i optimized. In the optimized setups, the height of the mirrors were adapted for each flight to maximize the isoplanatic angle. For fixed

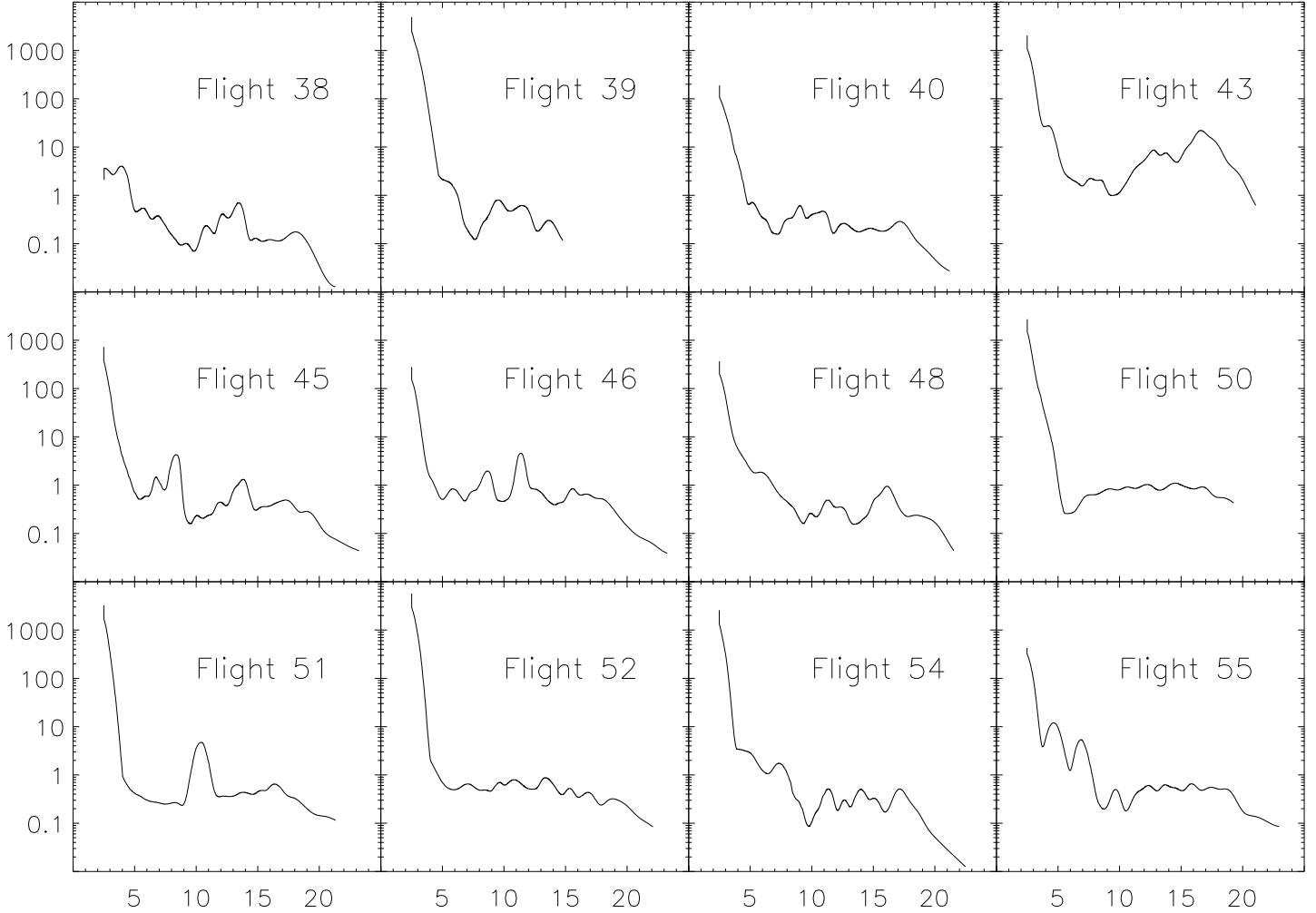


Figure 2. Profiles obtained by balloon soundings above Cerro Paranal, smoothed with a Gaussian of standard deviation 500 m. The abscissae are altitudes in kilometres above sea level. Ordinates are the refractive index structure constant (C_n^2) in units of $10^{-17} \text{ m}^{-2/3}$.

DMs, we chose the conjugation height as the median of the heights found by optimization. The DM configurations are summarized in Tab. 3, and our results are shown in Fig. 3.

With 3 DMs the increase in θ_3 (compared to θ_0) ranges from a factor of 2.6 to 13, depending on the profile. The median increase of θ_3 is a factor of 7.7, which means that the isoplanatic angle in the visible increases from $2.2''$ to $17''$. On particular nights (Flight 43 for example, which has a lot of extended high altitude turbulence) θ_3 stays small, $\sim 6''$. The largest θ_3 found was $28.9''$ (Flight 38). A wavelength of $2.2 \mu\text{m}$ yields a median θ_3 of $102''$ (for comparison, $\theta_0 = 13''$). A two mirror configuration brings improvement factors between 1.6 and 8.7, with a median of 4.6. Therefore, with 2 DMs, one can expect to increase the isoplanatic angle to $\sim 10''$ in the visible. Adapting the conjugate height of the DMs to profile variations is not crucial (θ_3 increases only by $\sim 7\%$ when using 3 optimized heights instead of fixed ones). Fig. 4 shows the optimal conjugate heights for the DMs as a function of flight number. Three main heights are identified: ground, $\sim 10\text{--}12$ km and $15\text{--}20$ km. Considering the observed stability of the optimum heights (due to the stability of the main turbulent layers), it is not surprising that optimizing the heights does not improve significantly

the FOV. Notice the large deviation for point 2 (Flight 39). As shown in Fig 2, the turbulence was located very low, and the balloon reached only a maximum altitude of ~ 15 km, leaving part of the turbulence unmeasured.

These results show that anisoplanatic effects occur in the visible even with 3 DMs used in an MCAO approach. They represent only one site, on a relatively short timescale. Other sites with similar isoplanatic angles exist (e.g. the measurements at Maidanak, Uzbekistan, provide a median θ_0 of $2.48''$ (Ziad et al. 2000)). Moreover, the θ_M computed here is somewhat pessimistic, since it contains a piston term (which reduces the isoplanatic angle but does not affect image quality) and does not take into account the finite number of corrected turbulent modes. This is similar to the effect seen with θ_0 , which overestimates isoplanatic effects (Chun 1998). Therefore, it is reasonable to expect a corrected FOV between $30''$ and $60''$ in diameter, in the visible. This is a considerable improvement over the few arcsecond isoplanatic field in the visible (roughly equal to θ_0), but much less than the tomographic FOV given by Eq. 1.

We suggest that the site where an ELT is built be optimized in terms of turbulence profiles, and not only total turbulence, as it used to be in previous surveys.

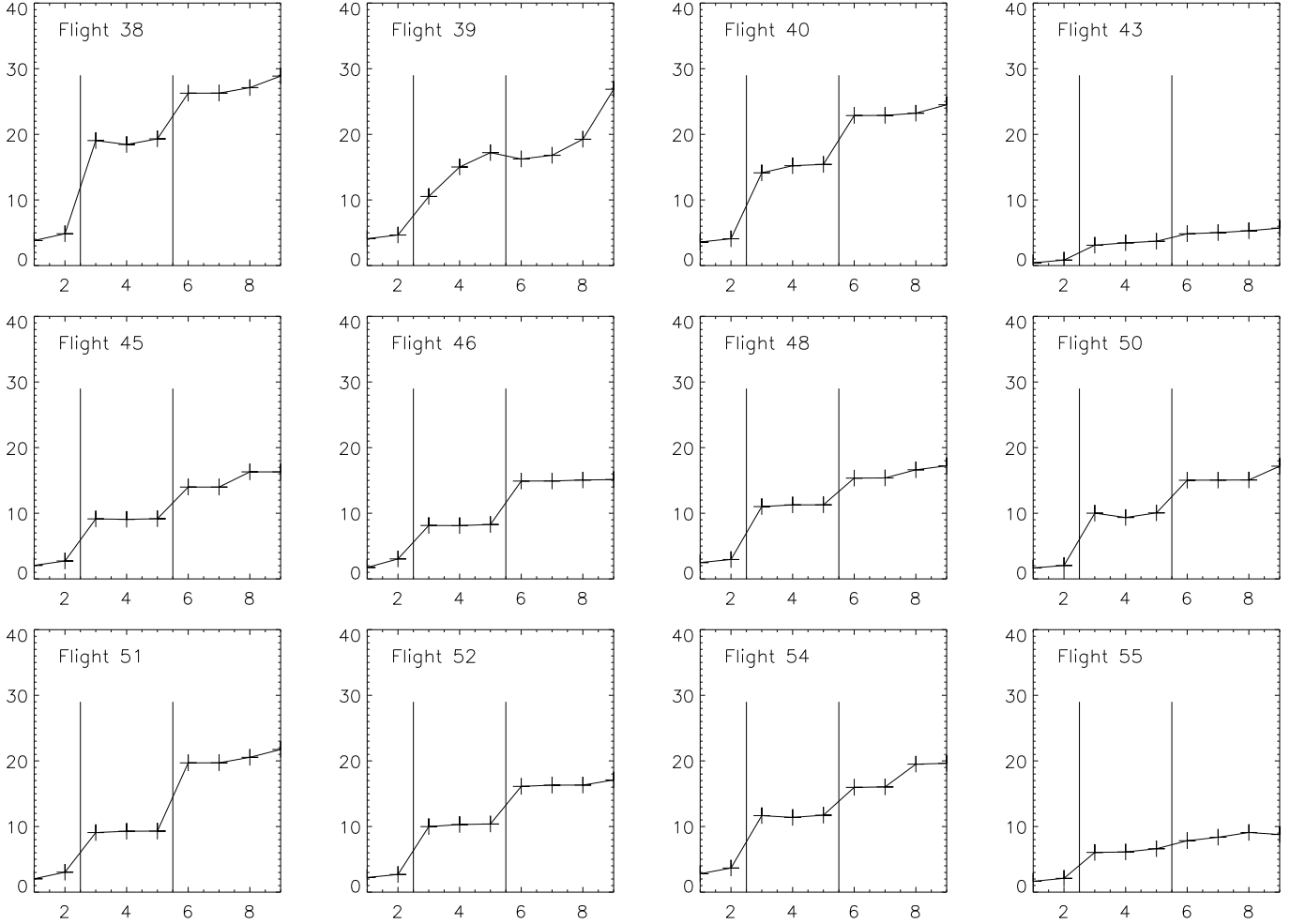


Figure 3. Isoplanatic angles (θ_M , ordinate axis, in arcseconds at $0.5 \mu\text{m}$) for different DM configurations (in abscissa, corresponding to N in Tab. 3). Configurations 1, 2 are for a single DM, 3 to 5 for 2 DMs and 6 to 9 for 3 DMs.

Table 3. MCAO configurations and optimization results for Cerro-Paranal. The columns contain: N – configuration number (same as in Fig. 3), M – number of DMs, H_1, H_2, H_3 – median conjugate heights of the DMs above sea level, θ_M – median isoplanatic angle in arcseconds at $0.5 \mu\text{m}$, G – gain in θ_M compared to the median θ_0 , G_{min} – minimum gain in θ_M , G_{max} – maximum gain in θ_M .

N	M	H_1, m	H_2, m	H_3, m	$\theta_M, ''$	G	G_{min}	G_{max}
1	1	F: 2638	-	-	2.20	1		
2	1	O: 5722	-	-	3.04	1.27	1.14	1.98
3	2	F: 3705	F: 15337	-	10.00	4.50	1.39	8.55
4	2	F: 3381	O: 15337	-	10.30	4.63	1.55	8.29
5	2	O: 3705	O: 15337	-	10.38	4.66	1.66	8.68
6	3	F: 3381	F: 10875	F: 17922	15.96	7.17	2.17	11.80
7	3	F: 3381	F: 10875	O: 18030	16.04	7.20	2.25	11.80
8	3	F: 3381	O: 11041	O: 17842	16.61	7.46	2.38	12.18
9	3	O: 3381	O: 10875	O: 17922	17.23	7.74	2.56	12.97

O – optimized altitude, maximizing the isoplanatic angle
 F – fixed altitude, taken to be the median of the optimized heights

It is more effective to correct a few strong layers (even if the total turbulence is higher), than a continuous repartition of lower amplitude turbulence. Indeed, comparing for example Flights 46 and 55 shows that a similar $\theta_0 \sim 1.7''$ can be well corrected with 3 DMs (Flight 46, $\theta_3 \sim 14''$) if turbulence is concentrated in a few peaks (see Fig. 2), whereas a quasi-continuous turbulence benefits much less from MCAO

correction (Flight 55, $\theta_3 \sim 9''$). The location of the turbulent layers should also be as stable as possible, to minimize the changes in DM conjugate height. Of course, some other parameters of the site will have impact on the telescope performance, like the wind (which is likely to be an important factor on such a large structure).

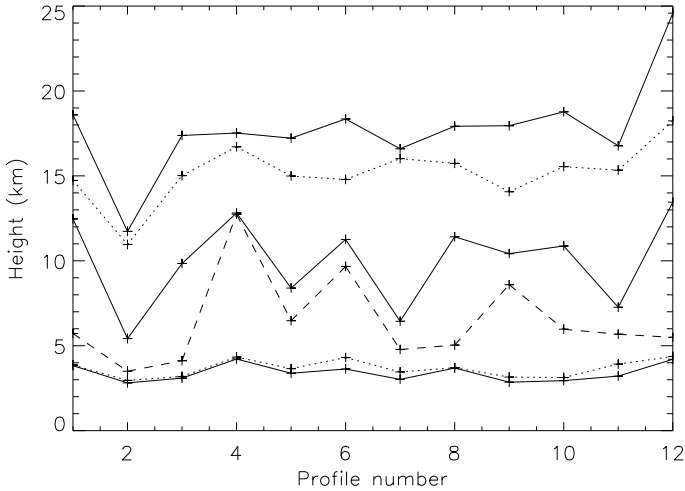


Figure 4. Optimized conjugate heights of the DMs (in kilometres) as a function of profile number. Solid line is for the 3 DM configuration, dots for the 2 DM configuration and dash is for a single DM

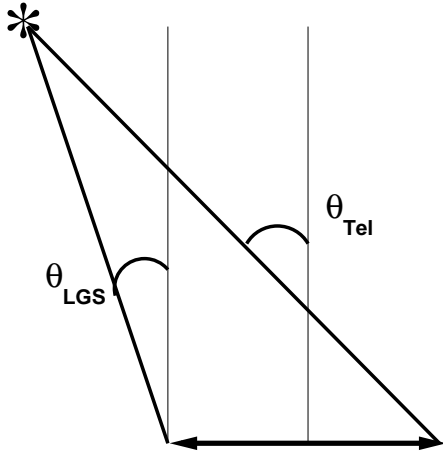


Figure 5. Required telescope field of view θ_{tel} compared to the corrected field θ_{LGS} which corresponds to the positions of the LGS. The need for a FOV much larger than θ_{LGS} is evident.

4.3 Required field of view

In tomographic wavefront sensing using LGSs the reference sources are placed at the edges of the corrected field (TF90). Therefore with 3 DMs the LGSs are positioned $\theta_{LGS} = \theta_3$ apart. The telescope FOV, θ_{tel} , must however be larger (see Fig. 5) for the laser spots to be imaged by the telescope:

$$\theta_{tel} = \theta_{LGS} + \frac{D}{H}. \quad (5)$$

For a 100 m telescope and a sodium LGS placed at a 90 km height, and for $\theta_{LGS} = 60''$, we get $\theta_{tel} = 290''$, or almost $5'$ in diameter. This can be a severe requirement for the telescope optical design.

5 NATURAL GUIDE STARS FOR VISIBLE CORRECTION

The use of several NGSs on an ELT to increase the corrected FOV and to find reference stars outside the isopla-

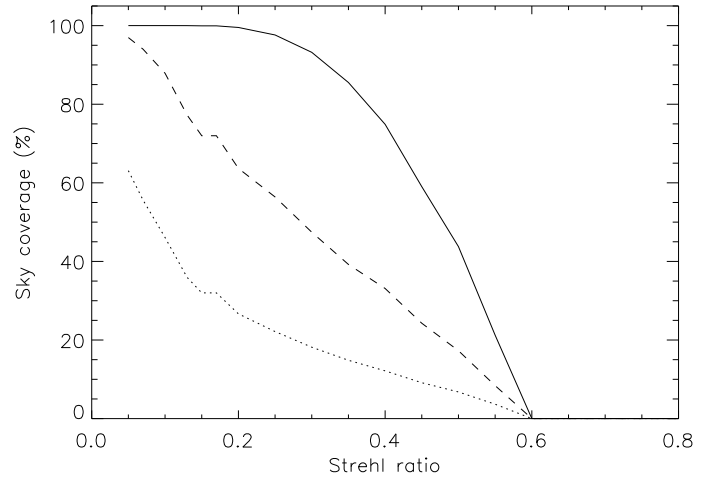


Figure 6. Sky coverage at $0.5 \mu\text{m}$ using 3 NGSs in a corrected FOV of $12'$ in diameter if wavefront sensing can be done in open-loop. From top to bottom curve: near Galactic plane, average Galactic latitude, near Galactic pole.

natic patch was proposed by Ragazzoni (1999). He pointed out that with turbulence tomography the maximum FOV which can be corrected increases linearly with telescope diameter, as shown by Eq. 1. Therefore, it would be possible to use the huge tomographic FOV to search for natural references. This work assumed that anisoplanatism was not present in turbulence tomography (turbulence concentrated in a few thin layers). In the previous paragraph we have shown that this is unfortunately not the case with real turbulence profiles. As a consequence, if the reference stars are much further away than θ_M they will not benefit from AO correction. The wavefront measurement would therefore be done in open-loop. This is a very unusual situation in AO (Roddier 1999), and experiments must be carried out to verify the feasibility of that approach.

Moreover, our further studies show that for widely separated NGSs, the errors of tomographic wavefront reconstruction with real turbulence profiles can be very high. So the use of 3 NGSs in a wide tomographic field seems problematic. Still, we estimate the sky coverage for this option.

Another constraint comes from the telescope design. The telescope FOV of an ELT is a strong cost driver and, at the moment, a full tomographic FOV ($17'$) does not seem to be feasible. Current optical designs for a 100 m telescope (Dierickx et al. 1999) provide a maximum FOV of $12'$.

We have computed the sky coverage (SC) for the case when reference stars are sought within a $12'$ FOV (Fig. 6). Full SC is obtained only near the Galactic plane. A 60 % SC can be achieved with a SR of 0.2 at average Galactic coordinates ($l = 180^\circ$, $b = 20^\circ$), or 30 % near the pole.

If a telescope design can be improved to have the maximum FOV allowed by tomography (Eq. 1) the SC will be significantly increased. A full SC can be achieved with a SR of 0.1 everywhere. SC of 50 % is achieved on the whole sky with a SR of at least 0.4. Given the performance of the AO system shown in Fig. 1, the telescope FOV size is identified here as a limiting factor for the sky coverage.

Initially we presumed in these simulations that the limiting magnitude for 3 NGSs is the same as for one NGS, e.g. $R \sim 10$ (Fig. 1). This is conservative with regards to the re-

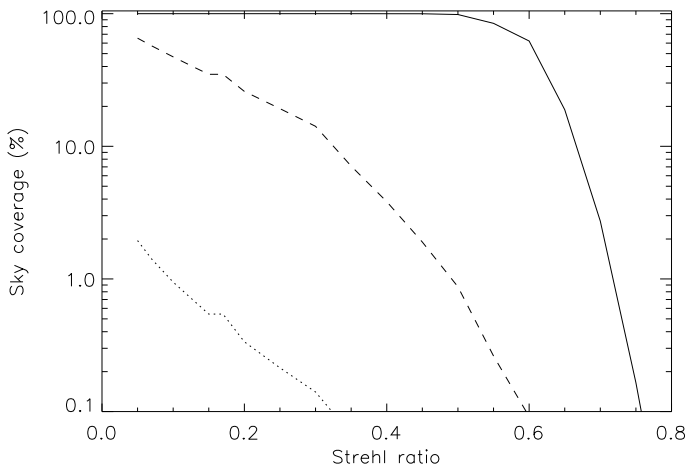


Figure 7. Sky coverage in the J band using 3 NGSs with a corrected FOV of $3'$ in diameter. From top to bottom curves: near Galactic plane, average latitude, near Galactic pole. Notice the logarithmic scale of the ordinate axis.

sults obtained by Johnston & Welsh (1994): when using four reference stars, the flux from the individual reference sources could be divided by four, i.e. a gain of 1.5 magnitudes. We have therefore also studied the cases where the limiting NGS magnitudes were one and two magnitudes fainter. Such gains could be achieved by efficient tomographic reconstruction algorithms. If the limiting magnitude can be increased by one magnitude, a SC of 40 % at the Galactic pole and 90 % at average Galactic latitudes can be obtained with a SR of 0.2. With the maximum tomographic FOV, a SC of 50 % is obtained with a SR 0.5 at the Galactic pole.

6 NATURAL GUIDE STARS AND CORRECTION IN THE INFRARED

The main problem of the NGS approach in the visible is caused by residual anisoplanatism. This problem is alleviated when only correction in the infrared is needed. At $1.25 \mu\text{m}$ θ_M is increased by a factor of 3 compared to the visible (see Eq. 2). For $\sim 60''$ FOV in the visible (diameter), a $3'$ corrected FOV is obtained. The limiting magnitude, as shown by Fig. 1, increases from $R \sim 10$ to $R \sim 13$. The sky coverage is plotted in Fig. 7. It shows that with a Strehl ratio of 0.2, SCs of 0.4 %, 30 %, 100 % are obtained respectively at Galactic poles, at average latitudes and in the Galactic disk. If a 1^m gain in limiting magnitude is obtained compared to a single NGS, the coverages increase only slightly.

At $2.2 \mu\text{m}$, the FOV is $\sim 6'$ (diameter), the limiting magnitude is about $R \sim 15$. The sky coverage is 10 % at the Galactic pole and complete elsewhere.

7 LASER GUIDE STARS

For astronomical AO systems LGSs based on resonant scattering in the sodium layer (Foy & Labeyrie 1985) are usually considered because they provide the highest reference source available, reducing the cone effect (also called focus isoplanatism, Foy & Labeyrie 1985, Fried & Belsher 1994, Tyler 1994). This effect is due to the finite altitude of the

laser guide star. It prevents obtaining high AO correction in the visible already with 8 m telescopes.

7.1 Power requirements

The laser power requirements for current AO systems working in the near-IR is of about 5 W (Continuous-Wave, CW), providing LGS brightness equivalent to a $\sim 9^m$ guide star (Jacobsen et al. 1994; Max et al. 1997; Davies et al. 1998). The typical sub-aperture size for those systems is 60 cm. Scaling to the subaperture size in the visible (16 cm) to obtain similar performance, the power of the laser should be 14 times higher (assuming a linear scaling of the guide star brightness with laser power), or about 70 W (CW). This scaling does not take saturation of the sodium layer into account. Milonni et al. 1998 provide an analytical tool to compute the power requirement in the case of a pulsed laser for a given guide star brightness with saturation. Using pulsed laser characteristics of the Keck LGS implementation (Sandler 1999) – 11 kHz repetition rate, 100 ns pulse duration, – we infer that to receive the same number of photons as for a 70 W CW laser, a ~ 175 W pulsed laser is needed. However, considering Fig. 1, we can see that a 9^{th} magnitude guide star would provide a Strehl ratio of 40 %. Therefore, if a slight loss of the AO system performance is acceptable, a significantly smaller amount of laser power would be sufficient.

One could instead use a Rayleigh-scattering based LGS system (Fugate et al. 1994). This has the advantage of being able to use any laser (producing a bright LGS at an arbitrary wavelength is currently not a problem, see Fugate et al. 1994). However, the low altitude of Rayleigh LGSs (~ 15 km) reduces its suitability for tomography. The position of the LGSs to obtain a zero corrected FOV (only the cone effect is removed) is:

$$\theta_{null} = \frac{D}{H}. \quad (6)$$

$\theta_{null} \sim 23'$ ($D = 100$ m, $H = 15$ km), whereas the maximum tomographic FOV (Eq. 1) allowed by the highest turbulent layer (10 km, optimistic considering Fig. 2) is $\sim 11'$ (for a guide star placed at 15 km). Therefore, the cone effect can not be fully corrected with only 4 Rayleigh LGSs on ELTs and we will not consider this option in the remainder of this paper.

7.2 Multiple sodium laser guide stars

On a 100 m telescope the use of a single LGS is totally impossible because of the huge cone effect involved. The option of using multiple (4) sodium laser guide stars in a tomographic fashion has therefore been investigated. We should stress that LGSs are placed on the edges of the corrected FOV (TF90), and therefore the problem of open-loop wavefront measurements does not affect this approach (the required FOV is given by θ_M). The problem with LGSs in turbulence tomography is that the wavefront tilt cannot be obtained from the LGS (Pilkington 1987) and propagates into the global reconstructed wavefront. In addition to global tilt, other low order modes (like forms of defocus and astigmatism) have to be measured from an NGS located in the reconstructed FOV (Le Louarn & Tallon 2000). Elaborate

Table 4. Scaling of curvature sensor limiting magnitude from a 3.6 m telescope with a correction at $2.2 \mu\text{m}$ to a 100 m at $0.5 \mu\text{m}$. D_{100} is the 100 m telescope diameter, $D_{3.6}$ the 3.6 m diameter. r_0 is given in the visible (~ 0.2 m). $\lambda_{0.5}$ is the correction wavelength of the ELT, $\lambda_{2.2}$ the correction wavelength of the 3.6 m telescope. The factor 19 is the number of sub-apertures on both pupils.

Factor	Flux gain (mag)
Diameter $\propto (\frac{D_{100}}{D_{3.6}})^2$	+7
Coherence time $\propto (\frac{\lambda_{2.2}}{\lambda_{0.5}})^{6/5}$	-2
Measurement precision $\propto \frac{1}{19} (\frac{D_{100}}{r_0})^2$	+10
Required precision $\propto (\frac{D_{3.6}}{D_{100}} \frac{\lambda_{0.5}}{\lambda_{2.2}})^2$	-10
Total	5

techniques have been proposed to measure the tilt from the LGS (see e.g. Foy et al. 1995, Ragazzoni 1996). Unfortunately, real time correction has not been demonstrated. If tilt can be retrieved, this problem disappears and full SC is achieved.

To solve the problem of LGS tilt indetermination, we propose to use in conjunction with LGS a very low order wavefront sensor (for example a curvature sensor, Roddier et al. 1988) working on a faint NGS. The limiting magnitude with 19 sub-apertures (4 sub-apertures across the pupil) is currently of $R \sim 17$ (Rigaut et al. 1998) on a 3.6 m telescope, with correction at $2.2 \mu\text{m}$. In Tab. 4, we summarize the scaling factors to be taken into account to convert this limiting magnitude to that of a 100 m telescope with a correction in the visible. The limiting magnitude is $R \sim 22$. This scaling is only valid if compensation is done in the visible, so that wavefront sensing benefits from the AO correction (Rousset 1994). Otherwise, as shown by Rigaut & Gendron (1992), there is no gain in limiting magnitude for low order wavefront sensing on a large aperture compared to 4 m class telescopes.

We used a model of the Galaxy developed by Robin & Cr ez e (1986) to get the probability to find a star of a given magnitude within a given FOV. Considering the faint magnitudes this system will be able to use, we also took into account the density of galaxies in the sky. We used galaxy counts given by Fynbo et al. (1999), based on a combination of measurements from the Hubble Deep Fields (North and South (Williams et al. 1996)) and the ESO NTT deep field (Arnouts et al. 1999)). Near the Galactic pole galaxies become more numerous than stars for magnitudes fainter than $R \sim 22$. A bias may exist since not all of these galaxies can be used as a reference due to their size (a source size smaller than 4 mas was assumed in Tab. 4). However, usually, the fainter the galaxies the smaller they are. We have assumed that galaxies are distributed evenly in the sky. Poisson statistics give the probability to find a reference object for a given AO limiting magnitude.

In Fig. 8 the probability to find an NGS within a field of $30''$ in diameter is shown. The SC is $\sim 13\%$ for the Galactic pole at $R \sim 22$. A twice larger corrected isoplanatic angle ($60''$ in diameter, Fig. 9), yields a SC of 40% at the poles, 70% at average latitudes and 100% near the Galactic plane. Scaling the SR vs limiting magnitude of current curvature systems, we expect a SR between 0.2 and 0.4 for this reference magnitude. At a magnitude of $R \sim 22$, most of the

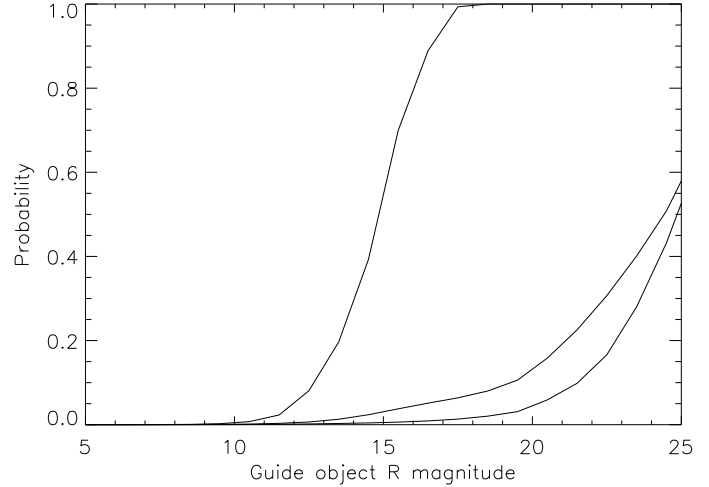


Figure 8. Sky coverage with 4-LGS, $\theta_3 \sim 30''$, top curve to bottom: Galactic center, average position and Galactic pole.

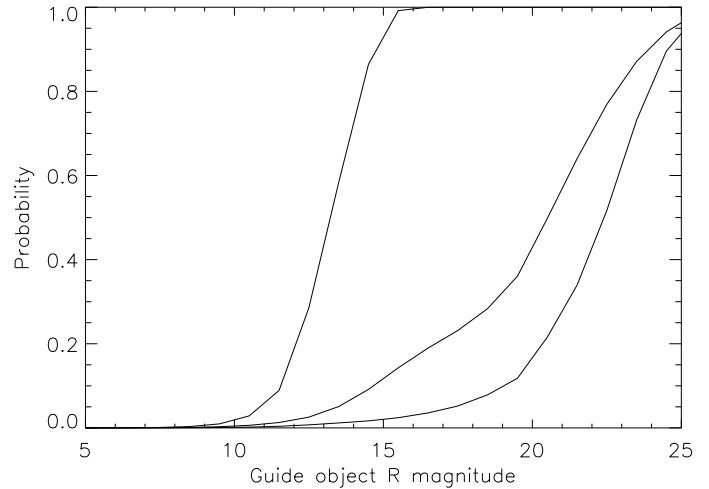


Figure 9. Sky coverage for the 4-LGS case, $\theta_M \sim 60''$, top curve to bottom: Galactic disk, average position and Galactic pole.

wavefront references sources will be galaxies when observing near the Galactic pole.

8 TECHNICAL CHALLENGES

In the previous sections, we have shown that there are no fundamental limitations imposed by the laws of atmospheric turbulence to building a visible light AO system on a 100 m optical telescope. In this section, we shall discuss the technical difficulties which have to be addressed to build such a system.

8.1 Wavefront sensor

The number of sub-apertures of the wavefront sensor impose the use of a large detector. Centroiding computations require at least 2×2 pixels per sub-aperture. For 16 cm sub-apertures, this means that the wavefront sensor detector must have at least 1250^2 pixels. Moreover, if guard pixels are used, this number could increase to 2500^2 (4×4 pixels

per sub-aperture). The pyramid wavefront sensor concept (Ragazzoni & Farinato 1999) requires only 2×2 per sampling area and therefore could be an interesting alternative to a SH sensor. The detector noise requirement could be loosened slightly from the $1e^-$ level we have used, if bright LGSs can be created in the atmosphere. This is however unlikely, since saturation problems in the sodium layer will arise (see section 7.1).

Currently, the state of the art detectors for wavefront sensors are 128^2 (Laurent et al. 2000). The required number of pixels could however be reduced by two means. One could use a curvature wavefront sensing method, coupled to a CCD detector. This approach has been proposed by Beletic, Dorn & Burke (1999) and has the advantage to reduce the number of pixels needed on the detector to one per sub-aperture. This would bring the total required number of pixels to $\sim 625^2$, which is realistic. It does not seem possible, with current technology, to produce a bimorph mirror (usually associated to curvature sensors) with 500000 actuators. This problem could be solved by coupling a curvature sensor to a piezo-stack deformable mirror but the approach clearly deserves more studies.

The read-out rate of the wavefront sensor detector (SH) can be obtained by scaling the typical current frame-rate in the IR (~ 200 Hz) to the visible. We obtain a frame rate of ~ 1.5 kHz. Therefore, there is a choice to be made between a smaller number of pixels but high frame-rate and a larger but slower system.

Both large number of pixels and high read-out speed can be achieved by butting small chips together, with multiple read-out ports (like in the Nasmyth Adaptive Optics System wavefront sensor, Laurent et al. 2000), or even more efficiently by adapting the CCD designing technique described in Beletic et al. (1999) to Shack-Hartmann systems, which allows a very efficient parallelization of the read-out process. Therefore the wavefront sensor detector should not be technically the most challenging part of the AO system.

8.2 Deformable mirror

With a typical DM diameter of 0.5 m which could be feasible on a 100 m telescope (Dierickx et al. 1999), the spacing requirement between the DM actuators would be 0.8 mm. This a value ten times smaller than on existing DMs. Therefore, the production of a DM with 500000 actuators clearly requires new methods. Current development based on MOEMS (Micro-Opto-Electro-Mechanical systems) could lead to spacings down to 0.3 mm, (e.g. Bifano et al. 1997, Vdovin et al. 1997, Roggeman et al. 1997) making possible a DM size of ~ 20 cm. One of the key issues in the design of these DMs is the required stroke. Assuming an outer scale of turbulence of 25 m and a von Kármán model, a stroke of $\pm 5 \mu\text{m}$ (3σ) would be sufficient. However, the actual turbulence spectrum at low spatial frequencies must be measured on 8 m class telescopes for realistic estimates of the required stroke.

8.3 Computing power

By using Moore's law, which states that the computing power doubles every 1.5 years, the computing power in 20 years will be increased by a factor of 10^4 .

Current wavefront computers have a delay smaller than 200 μs , which is compatible with use in the visible (Rabaud et al. 2000). The required computing power increase can therefore be estimated as the squared ratio of the number of controlled actuators:

$$\gamma = \left(\frac{N_{ELT}}{N_{IR-AO}} \right)^2, \quad (7)$$

where N_{IR-AO} is the number of actuators of current IR AO systems (200), and N_{ELT} the number of actuators for the ELT (500000). We get $\gamma \sim 6 \times 10^6$. However, this does not take into account that the cross-talk between actuators will be negligible for actuators far away from each other and therefore the interaction matrix will be very sparse. This will reduce significantly the computing load. If, for example, the interaction matrix (Boyer, Michaud & Rousset 1990) can be broken up into 6 times 100×100 matrices, the likely evolution in technology would bring the adequate power in 20 years.

Another possibility would be to use a curvature sensing, in which the interaction matrix is almost diagonal (if no modal control is employed), minimizing the computing power requirements. However, this approach, as noted earlier, seems to be prohibited by the availability of large bimorph mirrors.

8.4 Optics

The use of a small pitch between the actuators of the DM allows to maintain a small pupil diameter: with a pitch of 300 μm , the pupil size is 187 mm. This facilitates the imaging of the pupil on the wavefront sensor detector. Indeed, with 625 sub-apertures across the pupil, the WFS detector-size is roughly 25 mm (assuming 2 pixels per sub-aperture and 20 μm pixels). The reduction factor from the pupil to the detector is then 7.5, which is not a problem if each sub-aperture has a FOV of a few arcseconds.

Atmospheric dispersion (AD) correction is currently an unsolved problem and has to be tackled at the level of telescope design. For example, AD produces an elongation of the object of 184 mas (if AD is not corrected, assuming imaging between 0.5 and 0.6 μm , at a zenith angle of 30°) which is unacceptably high. The design of the AD corrector will be challenging, since an optimal combination of glasses, allowing a correction with an accuracy better than 1 mas must be found. The physical sizes of these AD correctors is also a problem, because of the large size of the optics. The required precision puts severe constraints on the measurement of atmospheric parameters (air temperature, humidity, pressure).

For the multi-NGS scheme this problem is even more crucial, since the NGSs must be far apart to increase the sky coverage, and will therefore suffer immensely from AD. The multi-LGS has the advantage to be insensitive to AD, because the sources are highly monochromatic.

If proper correctors cannot be built for technological reasons, narrow band operation of the telescope should be used if the highest spatial resolution is required: at 30° from zenith a bandpass of 0.4 nm produces a dispersion of ~ 1 mas, if no correction is made. The use of 3D detectors (like integral field spectrographs), would solve the problem, since images in different colors can then be disentangled.

In the multi-NGS case, if anisoplanatism limits the correction and the sources do not benefit from AO correction, non-common path aberrations between the sources will be difficult to maintain.

8.5 Laser spot elongation

The atmospheric sodium layer is roughly 10 km thick (e.g. Papen, Gardner & Yu 1996). This causes the LGS to be extended, for sub-apertures which are not on the optical axis of the telescope (assuming a projection of the LGS from behind the secondary mirror of the telescope). The apparent size of a laser spot is given by simple geometry:

$$\theta_{spot} \sim \frac{\Delta H d}{H_{Na}^2} \quad (8)$$

where ΔH is the thickness of the sodium layer (10 km), H_{Na} the altitude of the Sodium layer (≈ 90 km), d is the separation of the beam-projector and the considered sub-aperture. With $d=50$ m we get $\theta_{spot} \sim 13''$. Since the multiple LGSs will be off-axis, the spots will be even more elongated. This is clearly too large for standard wavefront sensors, which typically have a field of view of 2-3''. Several methods have been proposed to eliminate spot elongation. The conceptually simplest is to use a pulsed laser and to select only a small portion of the laser stripe by time gating the photons coming from the LGS. This has the advantage of being technically simple, at the cost of the effective brightness of the LGS. Other solutions have been proposed in the literature (e.g. Beckers (1992), improving the previous scheme by shifting the wavefront sensor measurements synchronously with the propagation of the beam in the sodium layer, thus removing the loss of photons at the price of complexity. Other less technically challenging solutions should certainly be investigated.

9 CONCLUSIONS

Although a realization of an adaptive optical system working with a 100 m telescope in the visible represents a technical challenge, it is shown here that very large aperture opens a number of new possibilities and such a correction becomes feasible for a significant fraction of the sky. The new approaches involve either use of several widely spaced bright NGS (in the near IR) or a very faint NGS combined with few LGS. In both cases a 3-D tomographic measurement of instantaneous phase screens is needed. Wavefront correction will be made with few (2-3) DMs conjugated to the optimum heights; in this way the FOV size is increased ~ 8 times compared to the single-DM AO systems, and FOV diameter may reach 1' in the visible. Additional criteria for site selection related to operation in this mode are formulated.

ACKNOWLEDGEMENTS

The authors would like to thank Roberto Ragazzoni for many useful discussions, Johan Fynbo for his data on the magnitude distribution of galaxies. This paper benefitted from many discussions with B. Delabre, Ph. Dierickx and R. Gilmozzi regarding the design of 100 m telescopes. We

Table 5. Summary of the studied systems. The system NGS (1) is based on 3 NGS with a wide FOV (6') to search for guide stars. The wavefront sensing is done in open loop. NGS (2) is also a 3 NGS system, but optimized for the near IR. The LGS stands for the 4-LGS system optimized for the visible.

	NGS (1)	NGS (2)	LGS
Wavelength (μm)	0.5	1.25	0.5
Strehl ratio (peak)	0.6	0.85	0.6
Max corrected FOV ⁽¹⁾	$\sim 60''$	3'	60''
Sky Coverage ⁽²⁾	60%	30%	70%
Number of NGS	3	3	1
Number of LGS	0	0	4
Technical difficulty	very high	low	medium

⁽¹⁾: Limited by residual anisoplanatism

⁽²⁾: with a Strehl ratio of 0.2, average Galactic latitude

are also grateful to an anonymous referee for improving the quality of this paper. This work was done with the help of the European TMR network "Laser guide star for 8-metre class telescopes" of the European Union, contract #ERBFMRXCT960094.

REFERENCES

- Andersen T., Ardeberg A., Beckers J., Flicker R., Gontcharov A., Owner-Petersen M., 1999, in Proc. of Workshop on Extremely Large Telescopes, Bäckaskog Castle, Sweden, June 1-2, 1999 (in press)
- Arnouts S., D'Odorico S., Cristiani S., Zaggia S., Fontana A., Giallongo E., 1999, *A&A*, 341, 641
- Azouit M., Vernin J., 1980, *J. Atmos. Sci.*, 37, 1550
- Beckers J. M., 1988, in ESO conference on very large telescopes and their instrumentation, Vol 2, pp. 693-703
- , 1992, *Appl. Opt.*, 31, 6592
- Beletic J. W., Dorn R. J., Burke B., 1999, in Proc. ESO workshop on Optical Detectors for Astronomy, Garching, September 1999, Amico P., Beletic J. W., eds., Kluwer Academic Publishers
- Bifano T. G., Mali R. K., Dorton J. K., Perreault J., Vandelli N., Horenstein M. N., Castanon D. A., 1997, *Opt. Eng.*, 36, 1354
- Boyer C., Michau V., Rousset G., 1990, *Proceedings of SPIE*, 1237, 406
- Chun M., 1998, *PASP*, 110, 317
- Coulman C. E., Vernin J., Fuchs A., 1995, *Appl. Opt.*, 34, 5461
- Davies R. I., Hackenberg W., Ott T., Eckart A., Holstenberg H.-C., Rabien S., Quirrenbach A., Kasper M., 1998, *Proceedings of SPIE*, 3353
- Dierickx P., Beletic J., Delabre B., Ferrari M., Gilmozzi R., Hubin N., Rigaut F., 1999, in Proc. of Workshop on Extremely Large Telescopes, Bäckaskog Castle, Sweden, June 1-2, 1999
- Foy R., Labeyrie A., 1985, *A&A*, 152, L29
- Foy R., Migus A., Biraben F., Grynberg G., McCullough P. R., Tallon M., 1995, *A&AS*, 111, 569
- Fried D. L., 1966, *J. Opt. Soc. Am.*, 56, 1380
- , 1982, *J. Opt. Soc. Am.*, 72, 52
- Fried D. L., Belsher J. F., 1994, *J. Opt. Soc. Am. A*, 11, 277
- Fuchs A., Vernin J., 1993, Final report on parca 1992 and 1993 campaigns. Tech. Rep. VLT - TRE - UNI - 17400 - 0001, ESO
- Fugate R. Q., et al., 1994, *J. Opt. Soc. Am. A*, 11, 310
- Fusco T., Conan J.-M., Michau V., Mugnier L. M., Rousset G., 1999, *Proceedings of SPIE*, 3762
- Fynbo J. U., Freudling W., Moller P., 1999, *A&A*, accepted
- Gilmozzi R., et al., 1998, *Proceedings of SPIE*, 3352, 778

- Graves J. E., Northcott M. J., Roddier F. J., Roddier C. A., Close L. M., 1998, *Proceedings of SPIE*, 3353, 34
- Jacobsen B., Martinez T., Angel R., Lloyd-Hart M., Benda S., Middleton D., Friedman H., Erbert G., 1994, *Proceedings of SPIE*, 2201, 342
- Johnston D. C., Welsh B. M., 1994, *J. Opt. Soc. Am. A*, 11, 394
- Laurent S., et al., 2000, *Proceedings of SPIE*, 4007 (in press)
- Le Louarn M., Foy R., Hubin N., Tallon M., 1998, *MNRAS*, 295, 756
- Le Louarn M., Tallon M., 2000, *J. Opt. Soc. Am. A*, in preparation
- Martin F., Tokovinin A., Ziad A., Conan R., Borgnino J., Avila R., Agabi A., Sarazin M., 1998, *A&A*, 336, L49
- Max C. E., et al., 1997, *Sci*, 277, 1649
- Milonni P. W., Fugate R. Q., Telle J. M., 1998, *J. Opt. Soc. Am. A*, 15, 217
- Mountain M., 1997, *Proceedings of SPIE*, 2871, 597
- Papen G. C., Gardner C. S., Yu J., 1996, in *OSA conf. on Adaptive Optics*, Vol. 13, pp. 96–99
- Pilkington J. D. H., 1987, *Nat*, 330, 116
- Rabaud D., et al., 2000, *Proceedings of SPIE*, 4007 (in press)
- Ragazzoni R., 1996, *A&A*, 305, L13
- , 1999, *A&AS*, 136, 205
- Ragazzoni R., Farinato J., 1999, *A&A*, 350, L23
- Ragazzoni R., Marchetti E., Rigaut F., 1999, *A&A*, 342, L53
- Rigaut F., Gendron E., 1992, *A&A*, 261, 677
- Rigaut F., Lai O., Rouan D., Salmon D., Arsenault R., Thomas J., Véran J. P., Gigan P., D. C., Fletcher J. M., Stilburn J., Boyer C., Jagourel P., 1998, *PASP*, 110, 152
- Robin A., Crézé, 1986, *A&A*, 157, 71
- Roddier F., 1981, in *Progress in optics*, Wolf E., ed., Vol. 19, Amsterdam, North-Holland Publishing Co., pp. 281–376
- Roddier F., ed., 1999, *Adaptive optics in astronomy*. Cambridge university press
- Roddier F., Roddier C., Roddier N., 1988, *Proceedings of SPIE*, 976, 203
- Roggeman M. C., Bright V. M., Welsh B. M., Hick S. R., Roberts P. C., Cowan W. D., Comtois J. H., 1997, *Opt. Eng.*, 36, 1326
- Rousset G. Adaptive optics for astronomy, Alloin D. M., Mariotti J.-M., eds., Kluwer Academic Publisher. pp. 115–137
- Sandler D. Adaptive optics in astronomy, Roddier F., ed., Cambridge university press. pp. 331–338
- Sarazin M., 1996, in *OSA/ESO topical meeting on adaptive optics*, Cullum M., ed., ESO/OSA, pp. 439–444
- Sasiela R. J., 1994, *Electromagnetic wave propagation in turbulence*, Brekhovskikh L., Felsen L., Haus H. A., eds. Springer-Verlag
- Stockman H. S., ed., *The Next Generation Space Telescope - Visiting a time when galaxies were young*, The Association of Universities for Research in Astronomy, Inc.
- Tallon M., Foy R., 1990, *A&A*, 235, 549
- Tallon M., Foy R., Vernin J., 1992, in *Progress in telescope and instrumentation technologies*, Ulrich M.-H., ed., ESO, pp. 517–521
- Tokovinin A., Le Louarn M., Sarazin M., 2000, *J. Opt. Soc. Am. A*, submitted
- Tyler G. A., 1994, *J. Opt. Soc. Am. A*, 11, 325
- Vdovin G., Middelhoek S., Sarro P. M., 1997, *Opt. Eng.*, 36, 1382
- Williams R. E., et al., 1996, *AJ*, 112, 1335
- Ziad A., Conan R., Tokovinin A., Martin F., Borgnino J., 2000, *Appl. Opt.*, in preparation

This paper has been produced using the Royal Astronomical Society/Blackwell Science L^AT_EX style file.